Global NEST Journal, Vol 20, No 1, pp 14-24

Ultrasound–assisted adsorption of toxic dyes by cottonseed cake: artificial neural networks, regression models and response surface optimization

Buyukada M.*, Evrendilek F. and Karakaya N.
Department of Environmental Engineering, Abant Izzet Baysal University, Bolu, Turkey
Received: 01/01/2017, Accepted: 02/03/2017, Available online: 23/01/2018
*to whom all correspondence should be addressed: e-mail: musabuyukada@hotmail.com

Abstract

In this study, dehydrated cottonseed cake as a low-cost and abundant byproduct in Turkey was utilized as an adsorbent for the decolorization of Reactive Blue 19 (RB19) and Reactive Yellow 145 (RY145) from aqueous solutions based on adsorption and ultrasound-assisted adsorption (UAA). Decolorization efficiency was optimized as a function of changes in process type, initial pH value, adsorbent concentration, temperature, reaction time, and initial dye concentrations of RY145 and RB19 based on response surface methodology (RSM) using Box-Behnken Design. The maximum decolorization efficiency of 99.9% for both RY145 and RB19 was obtained with ultrasound-assisted adsorption under the RSM-optimized conditions (with unity desirability) of 76.98 and 79.40 min reaction times, 233.20 and 254.29 mg L^{-1} initial dye concentrations, 1.37 and 1.44 g L^{-1} adsorbent concentrations, and 35.42 and 49.37 °C, respectively. The best-fit multiple non-linear regression models of decolorization efficiency with the highest adjusted coefficients of determination (R^2_{adj}) explained 99.52% and 99.48% of variations through adsorption of RY145 and RB19 and 98.14% and 98.01% of variations through UAA of RY145 and RB19, respectively, while artificial neural networks accounted for 99.82%.

Keywords: Adsorption; Data-driven modeling; Dehydrated cottonseed cake; Methylene blue; Ultrasound

1. Introduction

There exist thousands of commercially available dyes that are extensively used in such industries as pharmaceutics, leather, textile, paper printing, food, and cosmetics. However, these dyes when disposed also pose potential risks to public health and wildlife due to their such properties as low biodegradability, chemically complex structures, and toxicity (Sayan and Edecan, 2008; Tanyildizi, 2011). Thus, it is necessary for dyes to be removed from industrial wastewaters and effluents using innovative treatment techniques that are environmentally benign and economically feasible (Chen *et al*., 2015; Liu *et al*., 2015). Traditional treatment methods to achieve decolorization of wastewaters include chemical coagulation (Yang *et al*., 2011), electrochemical treatment (Sahinkaya, 2013), and biological treatment (Onat *et al*., 2010). However, these methods are often ineffective in decolorizing of complex dyes (Hamdaoui *et al*., 2008). Thus, advanced oxidation processes have gained popularity in the removal of dyes (Zhou *et al*., 2013). In particular, the applications of sonochemical adsorption such as ultrasound-assisted adsorption (UAA) to wastewaters laden with dyes, aromatic compounds, and/or chlorinated hydrocarbons have been showed to be an effective removal process for a wide range of dye wastewaters and effluents owing to its efficiency, flexibility and economic feasibility. Such UAA treatments cause the formation, growth, and sudden collapse of acoustic cavitation-induced micro bubbles in an irradiated liquid, thus leading to localized but high temperatures up to 5000 °C and hundreds of bars of pressures (Guo *et al*., 2011). Movement of liquid induced by sonic waves; that is, the conversion of sound to kinetic energy increases the rate of mass transfer near the surface (Guo *et al*., 2011).

Although activated carbon is the most commonly used adsorbent for the removal of dyes, exploring alternative low-cost adsorbents with a potential comparable to activated carbon is highly desired (Yang *et al*., 2011). Examples of such low-cost adsorbents used in wastewater treatment include peanut hull (Gong *et al*., 2015; Buyukada, 2016), sol meal hull (Arami *et al*., 2006), caol-based bottom ash (Dincer *et al*., 2007), bentonite (Korkut *et al*., 2010), wheat bran (Ozer and Dursun, 2007), tomato waste (Yargic *et al*., 2015), dead pine needles (Hamdaoui *et al*., 2008), sludge and straw (Ren *et al*., 2016), and wood sawdust (Ofamaja and Ho, 2008). Another low cost and abundant agricultural by-product is cottonseed (*Gossypium hirsutum*) cake (CC) obtained when cottonseed oil is extracted from cotton crops. Given the world's and Turkey's annual cottonseed productions of 46 and 1.3 million tons in 2014, respectively, CC appears to have a great potential to be used as an adsorbent in wastewater treatment about which there exist limited experimental studies.

On the other hand, optimization designs and data-driven modeling are the integral part of such scientific studies of

experimental nature as they are leveraged not only to maximize information extracted from data and minimize experimental random errors and runs but also to provide quantification, generalization, and thus, predictive power, respectively. Artificial neural networks (ANNs) and multiple non-linear regression (MNLR) models are the most commonly used tools to quantify and predict non-linear patterns and behaviors. Likewise, response surface methodology (RSM) is the most utilized design to determine optimum operating conditions to maximize or minimize non-linear response surfaces by taking into account second-degree interactions.

As is evident from the above introduction, the motivation behind the present study was threefold: increased efficacy of UAA, high potential of CC as an adsorbent, and empirical optimization and modeling as a leverage for a better understanding. The objective of this study was therefore to model and optimize decolorization efficiency for the two toxic dyes of Reactive Blue 19 (RB19) and Reactive Yellow 145 (RY145) through ANNs, MNLR models, and RSM optimization as a function of changes in process type (adsorption versus UAA), initial pH, initial CC and dye concentrations, temperature, and reaction time.

2. Materials and methods

2.1. Sampling and characterization of CC

Cottonseed cake was utilized as an adsorbent and was supplied from a local textile plant in Adana, Turkey. After being washed with deionized water for the removal of soluble impurities, CC samples were obtained after being dried in an oven (DV452, Chanel, China) at 80 °C for 24 h for the removal of moisture. Immediately after being grinded using a ball mill (Mertest LB 220, England), the CC samples were sieved to obtain various fractions, using American Society for Testing and Materials (ASTM) standard sieves. The CC samples were stored in a $CaCl_2$-desicator during the experimental study.

Specific surface areas of the CC samples were estimated from N_2 adsorption isotherm data obtained at 77 K using a BET surface analyzer (Micnometrics, ASAP 2020). Prior to N_2 adsorption isotherm experiments, CC was degassed at 131 °C (up to $1.33*10^2$ bar) for 6 h. Pore size distribution of CC was also calculated from N_2 adsorption isotherm, while particle size distribution of CC was obtained using a particle size analyzer (Malvern-Mastersizer 2000). Fourier Transform Infra Red (FTIR) spectrum of CC was obtained using a FTIR spectrometer (Matsson 1000 FTIR) based on the KBr pellet technique in the range of 400 to 4000 cm^{-1}. XRD analysis was carried out to determine organic matter type of CC, using a diffractometer (Multiflex–DD2759N, Rikagu, Japan) with Cu Kα radiation (λ = 1.568 Å). Zero point charge (pH_{zpc}) of CC was measured using a zeta potential meter (Zetasizer, 3000HSA, Malvern, UK). The surface morphologies and elemental mapping of CC were analyzed using a SEM–EDX (JSM–6390V, Jeol, Japan). Chemical composition of CC was analyzed using an X-ray fluorescence spectrometer (XRF, Thermoscientific Lumina).

2.2. Preparation of reactive dye solutions

The commercial azo dyes with the following Color Index generic names of Reactive Yellow 145 (RY145, $C_{28}H_{20}ClN_9O_{16}S_5Na_4$; molecular weight = 1026.26 g/mol; λ_{max} = 420 nm) and Reactive Blue 19 (RB19, molecular weight = 626.54 g/mol; λ_{max} = 592 nm) were obtained from a local textile firm in Corlu (Turkey) and used without further purification. The stock solutions of the reactive dyes were prepared in a constant concentration of 1.0 g/L and then diluted to appropriate concentrations. Working solutions of the desired concentrations were obtained using successive dilutions. The initial pH of each solution was adjusted to the required value with concentrated and diluted HCl and NaOH solutions before the experiments.

2.3. Experimental procedure

Batch sorption experiments were carried out in a 1000mL cylindrical jacketed vessel put on an overhead mechanical stirrer (IKA RW 20, Kutay Group, Turkey) which stirred the mixture at various agitation speeds. The mechanical stirrer was used to have well mixed suspension characteristics for the solid particles. Ultrasonic irradiation was chosen as one of the mandatory effects of the removal process and was obtained from a digital ultrasonic cleaner (WiseClean WUC–DH, Wisd, Germany) operating at the frequencies of 5 to 40 kHz and the ultrasonic powers of 16 to 344 W. The vessel was set in ultrasonic cleaner vertically. Total mixture volume was determined as 500 mL and the experiments were effectuated according to Box-Behnken Design (BBD) considering the previous experiments (Buyukada, 2015).

2.4. Spectrophotometric analysis

The solutions were analyzed at predetermined time intervals for the final concentrations of RY145 and RB19 using a UV/vis spectrophotometer (SHIMADZU UV-2100, Biomerieux, France) for the maximum absorbance value. Dye concentration was calculated from a calibration curve. Decolorization efficiency (DE, %) at any time was estimated as follows (Buyukada, 2015; Buyukada and Evrendilek, 2016a):

$$DE=\frac{C_0-C_t}{C_0}\times 100 \quad (1)$$

where C_o and C_t are the initial and measured concentration (mg L^{-1}) values of the samples at a specified interval during a four-hour reaction, respectively. Dye concentrations (C_{RY145} and C_{RB19}, mg L^{-1}) after each experiment were calculated using the best-fit calibration plot (absorbance expressed in IU = $0.0189*C_{RY145}$; R^2 = 0.99; p < 0.001; A = $0.0161*C_{RB19}$; R^2 = 0.99; p < 0.001).

2.5. Empirical modeling

120 experiments were performed totally with three replicates considering the Box-Behnken design schedule. Effects of six explanatory variables of adsorbent concentration (AC, 0.5 – 1.5 g L^{-1}) (1), initial dye concentration (IDC, 225 – 375 mg L^{-1}) (2), reaction time (RT, 30 – 120 min) (3), temperature (T, 25 – 50 °C) (4), process type (PT, ads and UAA) (5), and dye type (DT, RY145 and RB19) on color removal efficiency (DE, %) were investigated

experimentally and statistically. Design Expert 9.0.6 (Statease), Minitab 17 (Minitab, Inc., State Collage, PA), and Matlab 2012b (Matworks Inc.) were used to apply RSM and develop MNLR models and ANNs, respectively. The stepwise procedure was used to choose the best-fit MNLR models with the highest goodness-of-fit measured by adjusted coefficient of determination (R^2_{adj}), and the highest predictive power measured by coefficient of determination based on leave-one-out cross-validation (R^2_{CV}). All the predictor variables were treated as the categorical variables in the RMS optimization. The process type of adsorption versus UAA was incorporated in the MNLR models as a categorical variable with adsorption being held as the baseline. Variance inflation factor (VIF) for multicollinearity and Durbin-Watson (DW) statistics for autocorrelation were reported with the best-fit MNLR models (Buyukada, 2017). The parametric test assumptions of normality and constant variance were also tested during the implementation of one-way analysis of variance (ANOVA) and MNLR. Tukey's multiple comparison test following ANOVA at a confidence interval of 95% was used to detect the significant differences in decolorization efficiency among the explanatory variables.

In this study a single-layer perception (SLP) was used to predict decolorization efficiency based on feedforward Gradient descent with momentum (GDX), adaptive learning rate, and backpropagation algorithm. GDX is not a commonly used model such as Levenberg-Marquardt (LM), and Quasi-Newton (BFG) because of its high iteration time. The SLP network consisted of inputs, and hidden and output layers connected by weights and biases. The input layer included the following four neurons: (1) adsorbent concentration (for all the processes), (2) temperature (for adsorption only) and frequency (for UAA only), (3) reaction time (for all the processes), and (4) initial dye concentration (for adsorption only) and ultrasonic power-dependent weight loss ratio (for UAA only).

Hidden layers were used to solve the complex non–linear functions on the ANNs. The number of neurons in the hidden layers, and training epochs were selected by trial and error. Training and independent validation performances of the ANNs were determined considering root mean square error (RMSE) in Eq. (2) and mean absolute error (MAE) in Eq. (3). An ANN model with the highest R^2 value and the lowest RMSE and MAE values were selected as the best-fit ANN model according to independent validation data.

$$RMSE=\sqrt{\frac{1}{N}\left(\sum_{i=1}^{N}(O_i-P_i)^2\right)} \quad (2)$$

$$MAE=\frac{1}{N}\left(\sum_{i=1}^{N}|O_i-P_i|\right) \quad (3)$$

where O_i and P_i are observed and predicted values, respectively.

3. Results and discussion

3.1. Characterization of CC

The chemical composition of CC obtained from XRF analysis is presented in Table 1. Its main components included organic carbon, cellulose, hemicelluloses, and lignin.

The FTIR spectra of CC illustrated in Fig. 1 showed bonded hydroxyl groups (phenolic and alcoholic groups) at 3350 cm^{-1}, C–H vibrations (non-ionic carboxyl groups) at 2750 cm^{-1}, C=O vibrations (carboxyl groups) at 1750 cm^{-1}, C=C vibrations (aromatic rings) at 1550 cm^{-1}, C–H vibrations (phenol groups) at 1250 cm^{-1}, and C–O vibrations (ether groups) at 1150 and 1070 cm^{-1}.

Table 1. Chemical composition of dehydrated cottonseed cake (CC)

	Compound	Value (wt %)
As received	Moisture content	5.7
	Cellulose	28.6
	Oil content	7.3
Dry weight (%)	Proximate analysis	
	Ash	5.2
	Volatile matter	80.6
	Fixed carbon*	8.9
Dry weight on ash-free basis (%)	Ultimate analysis	
	Organic C	53.1
	H	5.7
	N	1.2
	O*	41.4
	C/H	1.3

**Estimated by difference*

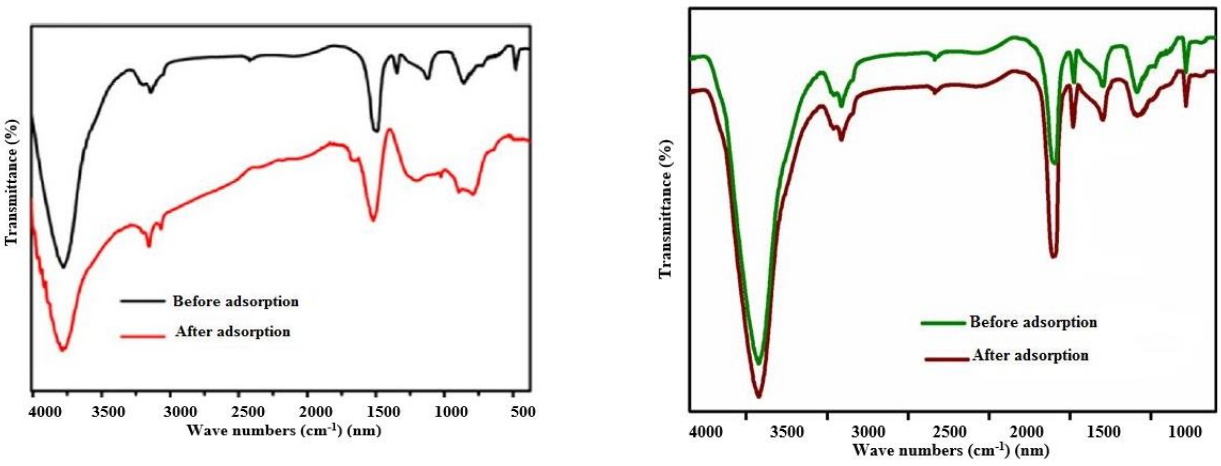

Figure 1. (a) FTIR spectrum of cottonseed cake (CC) before and after adsorption of RY145, (b) FTIR spectrum of cottonseed cake (CC) before and after adsorption of RB19

Fig. 2 also pointed to hydroxyl and amino groups of CC in a wide vibration range at 3400 cm^{-1} which decreased significantly with acid hydrolysis of CC. Mean surface area of CC according to the BET analysis were estimated at 26.7 $m^2 g^{-1}$, while the total pore volume of CC was determined as 0.253 $cm^3 g^{-1}$. N_2 adsorption isotherm and pore size distribution of CC are shown in Figure 2a. As can be seen from pore size distribution in Figure 2b, CC contained both micropores (< 25 Å) and mesopores (25 Å < pore width < 400 Å).

The physicochemical properties of CC are shown in Table 2.

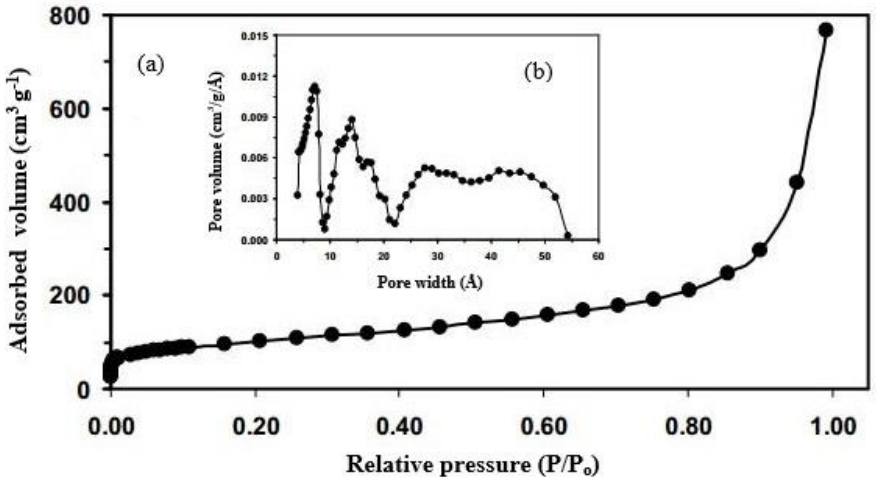

Figure 2. (a) BET surface area and (b) pore size distribution analyses of cottonseed cake (CC)

Table 2. Physicochemical properties of dehydrated cottonseed cake (CC)

Physicochemical properties	Value
Density (picnometric method, g cm^{-1})	1.683
Specific surface area ($m^2 g^{-1}$)	4.72
Zeta potential (pH_{zpc})	5.12

According to the particle size distribution analysis illustrated in Figure 3, the size of CC particles was lower than 50 mesh. In addition, the maximum volume was observed in the particle size of 100 mesh.

3.2. Linear effects of operating conditions

A positive correlation was found between reaction time and decolorization efficiency through adsorption (r = 0.454, p = 0.011) and UAA (r = 0.472, p = 0.009) (Fig. 4). Consistent with our findings, the increased reaction time was also reported to increase decolorization efficiency through

many wastewater treatment processes (Mall *et al*., 2006). The extended duration of reaction time was most likely to contribute to a long equilibrium time of the removal process that resulted in increased decolorization efficiency.

The increased initial dye concentration decreased decolorization efficiencies through both adsorption and UAA. This negative correlation between initial dye concentration and decolorization efficiency is illustrated in Figure 4a and c for the adsorption process (r = -0.612; p < 0.01) and in Figure 4b and d for the UAA process (r = -0.624; p < 0.001). The decreased decolorization efficiency, and the equilibrium time were attributed in the related literature to the increased amount of organic effluent in mixture medium (Mall *et al*., 2006).

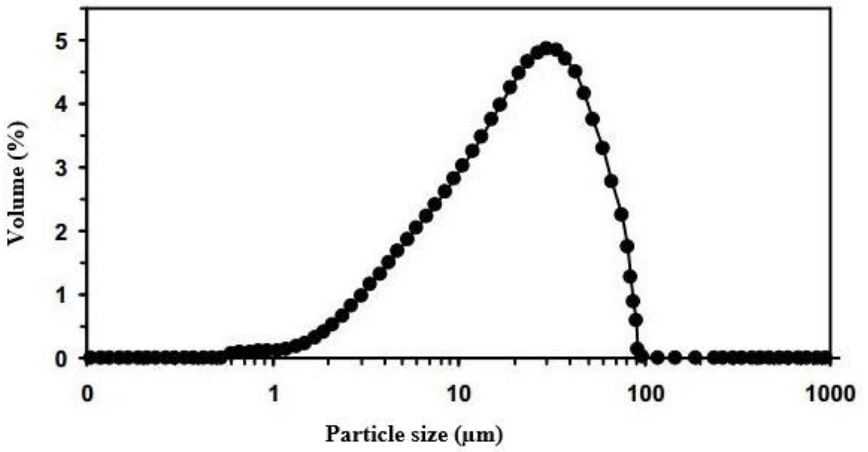

Figure 3. Particle size distribution of cottonseed cake (CC)

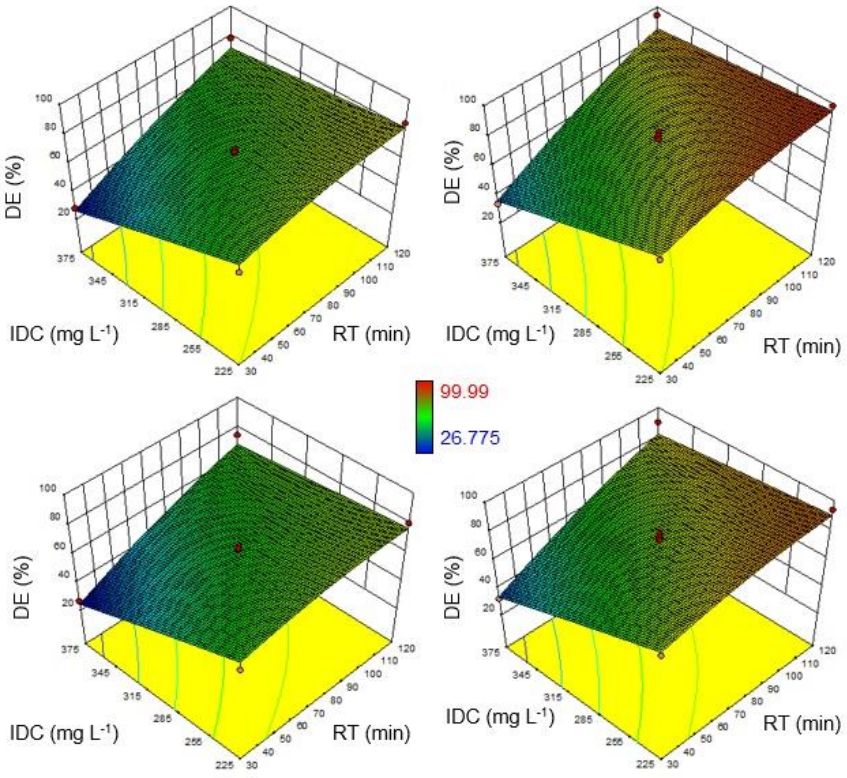

Figure 4. Interaction effects of initial dye concentration (IDC, mg $L^{-}1$) by reaction time (RT, min) on decolorization efficiency (DE, %) through (a) adsorption and (b) ultrasound-assisted adsorption (UAA) of RY145 and (c) adsorption and (d) UAA of RB19 under 37.5 ^{o}C and 1.0 g L^{-1} CC concentration

Temperature was found as the least significant predictor of decolorization efficiency regardless of the process type (p = 0.03). A positive correlation was found between temperature and decolorization efficiency through adsorption (r = 0.112; p = 0.032) and UAA (r = 0.121; p =

0.028). Likewise, Mall *et al*. (2006) found increased temperature to lead to increased decolorization efficiency.

Increased quantity of adsorbent in the mixture medium resulted in an increase in decolorization efficiencies through both processes. The strength of the positive correlation between adsorbent concentration and decolorization efficiency gave *r* values of 0.522 through adsorption (p = 0.002) and 0. 573 through UAA (p = 0.001). Similar results were also obtained in the study by Mohan *et al*., (2002).

3.3. Interaction effects of operating conditions

According to our ANOVA results, impacts of the following four interaction terms were found significant on the decolorization efficiencies via both adsorption and UAA: (1) initial dye concentration by reaction time (p < 0.001), (2) initial dye concentration by temperature (p < 0.001), (3) initial dye by adsorbent concentrations (p = 0.001), and (4) the quadratic effect of initial dye concentration (p < 0.0001*)*. Similar results were obtained in related literature (Sayan and Edecan, 2008; Hamdaoui *et al*., 2008; Buyukada and Evrendilek, 2016ab). Interaction effects of initial dye concentration by reaction time through adsorption and UAA are illustrated in Figure 4. Our results also showed that all the linear effects of the explanatory variables were significant on the decolorization efficiencies through adsorption and UAA (Table 3).

Table 3. Analysis of variance (ANOVA) results of response surface methodology (RSM) using Box Behnken Design (BBD)

Source	Sum of Squares	df	Mean Square	*F* Value	*p* value
Model	31527.40	25	1322.18	81.23	< 0.0001
RT	10852.40	1	10852.40	666.71	< 0.0001
IDC	7936.72	1	7936.72	487.59	< 0.0001
CC	4565.24	1	4565.24	280.46	< 0.0001
T	1869.71	1	1869.71	114.86	< 0.0001
PT	4013.82	1	4013.82	246.59	< 0.0001
DT	363.37	1	363.37	22.32	< 0.0001
RT*IDC	1172.18	1	1172.18	72.01	< 0.0001
RT*CC	8.22	1	8.22	0.51	0.4790
RT*T	56.65	1	56.65	3.48	0.0652
RT*PT	52.58	1	52.58	3.23	0.0755
RT*DT	6.51	1	6.51	0.40	0.5285
IDC*CC	267.81	1	267.81	16.45	0.0001
IDC*T	720.62	1	720.62	44.27	< 0.0001
IDC*PT	0.00677	1	0.00667	0.00042	0.9838
IDC*DT	4.76	1	4.76	0.29	0.5898
CC*T	0.17	1	0.17	0.011	0.9185
CC*PT	1.34	1	1.34	0.082	0.7748
CC*DT	2.74	1	2.74	0.17	0.6825
T*PT	1.36	1	1.36	0.084	0.7732
T*DT	1.12	1	1.12	0.069	0.7934
RT^2	2.41	1	2.41	0.15	0.7013
IDC^2	285.56	1	285.56	17.54	< 0.0001
CC^2	1.90	1	1.90	0.12	0.7337
T^2	10.11	1	10.11	0.62	0.4326
Residual	705.28	1	705.28	43.33	< 0.0001
Lack of fit	3.09	94	6.28	0.36	0.5228
Pure error	1375.02	74	18.58	2.40	0.0153
Total	155.07	20	7.75		

CC: Adsorbent concentration (g L^{-1}); DE: Decolorization efficiency (%); df: degrees of freedom; DT: Dye type; IDC: Initial dye concentration (mg L^{-1}); PT: Process type; RT: Reaction time (min); and T: Temperature (°C).

3.4. Effect of ultrasound

Enhanced adsorption may be due to altered equilibrium time and improved adsorption kinetics. Ultrasonic energy may shift the adsorption equilibrium to a new one (Hamdaoui *et al*., 2008). Ultrasound may also increase adsorption rate by accelerating mass transfer due to hydro dynamical effects generated by acoustic cavitation (Buyukada and Evrendilek, 2016b). Micro jets and shockwaves produced by cavitation can disrupt the adsorbent structure and lead to a higher adsorption capacity. Enhanced decolorization of dyes was also reported to stem from thermal properties induced by localized hot spots formed when bubbles were cavitated (Hamdaoui *et al*., 2008; Buyukada and Evrendilek, 2016b). The significant and positive effect of ultrasound on color removal efficiency was illustrated in Figure 5 and 6. As it was seen from these figures, ultrasound leaded an increase in color removal efficiency.

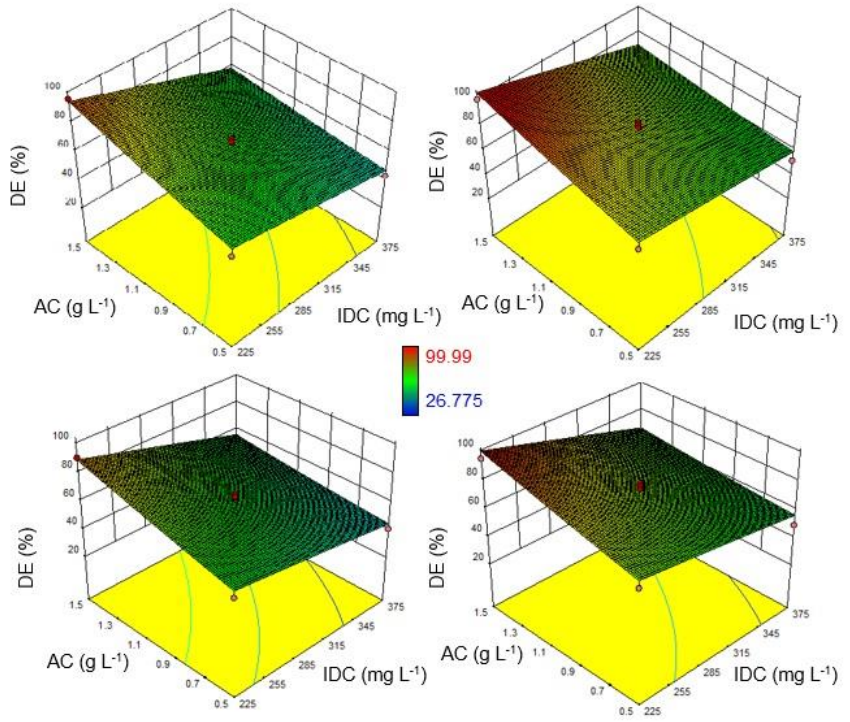

Figure 5. Interaction effects of initial dye concentration (IDC, mg L-1) by adsorbent concentration (AC, g L^{-1}) on decolorization efficiency (DE, %) through (a) adsorption and (b) ultrasound-assisted adsorption (UAA) of RY145 and (c) adsorption and (d) UAA of RB19 under 37.5 °C and 75 min of reaction time

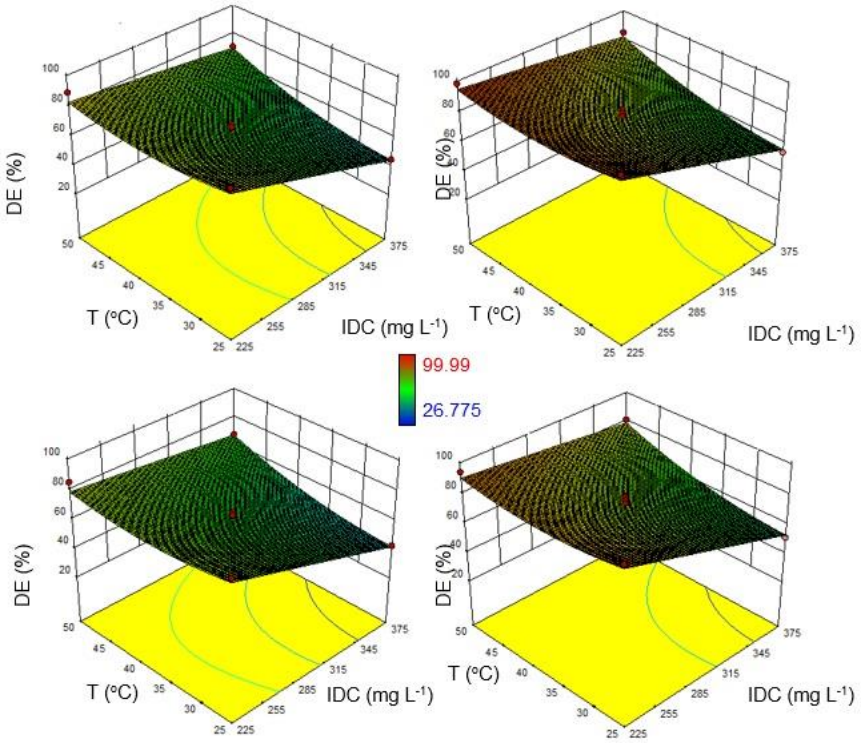

Figure 6. Interaction effects of initial dye concentration (IDC, mg L-1) by temperature (T, °C) on decolorization efficiency (DE, %) through (a) adsorption and (b) ultrasound-assisted adsorption (UAA) of RY145 and (c) adsorption and (d) UAA of RB19 under 75 min of reaction time and 1.0 g L^{-1} CC concentration

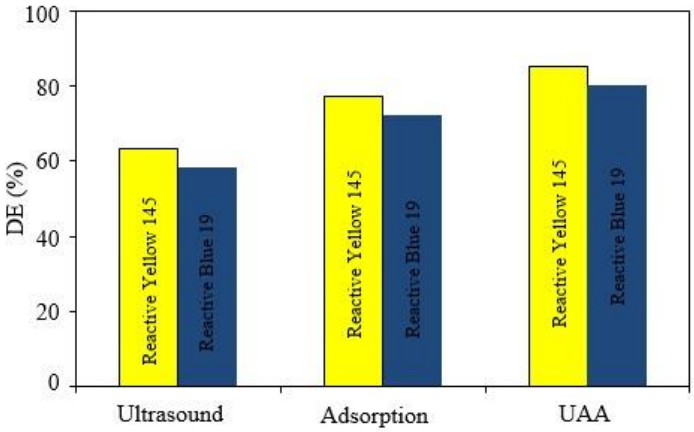

Figure 7. Effects of adsorption, ultrasound, and ultrasound-assisted adsorption (UAA) on decolorization efficiency (DE, %)

Another statement of significant effect of ultrasound on adsorption efficiency was illustrated in Figure 7.

As a result, both rate and amount of adsorption significantly increased with the presence of the UAA process owing to sonication-enhanced removal of the dyes through the extreme conditions generated by cavitation bubbles. UAA-induced decolorization efficiency of 99.9% in 5 min can be attributed to the strong convective currents occurring within the reactor. These effects associated with the hydrodynamic phenomena due to cavitation and mechanical stirring are responsible for the perfect mixing of the vessel content. Thus, the vessel used under the ultrasonic irradiation appeared to be a completely stirred tank reactor which was in close agreement with results of similar studies (Hamdaoui *et al.*, 2008; Buyukada and Evrendilek, 2016b).

3.5. Empirical models

The best-fit MNLR models of decolorization efficiencies through adsorption and UAA for RY145 and RB19 are presented in Table 4. The most important explanatory variable regardless of the process type was the initial CC concentration given the magnitude of its coefficient. The quadratic and interaction terms of the explanatory variables were significantly influential on the decolorization efficiencies. R^2_{adj} of 99.48% and R^2_{cv} of 97.52% were found for adsorption of RB19, while R^2_{adj} of 98.01% and R^2_{cv} of 96.52% were found for UAA of RB19. The following two types of ANNs were derived from the experimental data for RY145: single layer perception (SLP) and multilayer perception (MLP). SLPs had an input and only one hidden layer based on tangent sigmoidal, and an output layer based on linear. MLPs had an input and two hidden layers based on sigmoidal and an output layer based on linear.

A total number of 69 ANNs models were built and divided into the three groups: (1) SLPs with 3 to 25 neurons in the hidden layer, (2) MLPs with three neurons in the first hidden layer and 3 to 25 neurons in the second hidden layer, and (3) MLPs with five neurons in the first hidden layer and 3 to 25 neurons in the second hidden layer (Table 5). All the ANNs models were derived using Levenberg–Marquardt (TRAINLM) feedforward and backpropagation algorithms. Our results in Table 5 showed that the best-fit ANN45 model had RMSE of 2.04, MAE of 0.012 according to the highest predictive power (R^2 value of 98.57%) for the independent validation. The predictive power of the best-fit MNLR models was 97.79% for adsorption of RY145 and 96.61% for UAA of RY145 (Table 4), while that of ANNs ranged from 98.11% to 99.09% (Table 5). However, the ANN45 had the highest goodness-of-fit value (R^2_{adj} = 99.82%), while the best-fit MNLR models had R^2_{adj}values of 99.52% for adsorption of RY145 and 98.14% for UAA of RY145.

3.6. RSM optimization, validation and ANNs

The optimal operating conditions for the maximum decolorization efficiency of 99.99% were determined for both adsorption and UAA consistently thus: 119.99 and 76.98 min reaction times, initial MB concentrations of 225.41 and 233.20 mg L^{-1}, CC concentrations of 1.41 and 1.37 g L^{-1}, and 50 and 35.42 °C, respectively, for RY145 (Table 6). The reaction times of 120 and 79.40 min, initial MB concentrations of 226.50 and 254.29 mg L^{-1}, CC concentrations of 1.50 and 1.44 g L^{-1}, and 50 and 49.37 °C were determined as the optimal operating conditions with the maximum decolorization efficiency of 97.84% and 99.99% for adsorption and UAA, respectively, for RB19 (Table 6).

Following the development of the best-fit MNLR and ANN models, validation experiments were performed to test the RSM-optimized conditions. Based on the independent validation dataset, ANN45 had the highest R^2 value of 98.57% (Table 5). RSM-optimized conditions for the predicted and experimental decolorization efficiencies through adsorption and UAA of RY145 and RB19 are presented in Table 6. The validation process confirmed that the RSM optimization was successfully applied to the removal of RY145 and RB19 through the adsorption and UAA processes (Table 6).

Table 4. Multiple non-linear regression (MNLR) models of decolorization efficiency through adsorption and ultrasound-assisted adsorption (UAA)*

Categorical predictor	Coefficient	RY145		RB19	
		Adsorption	UAA	Adsorption	UAA
Constant	70.15	184.2713	192.3865	181.6553	189.2037
RT	15.04	-0.0454	0.0011	-0.0618	-0.0153
IDC	-12.86	-0.4970	-0.4973	-0.4886	-0.4889
CC	9.75	49.9592	49.2909	49.0034	48.3352
T	6.24	-3.8492	-3.8222	-3.8736	-3.8467
PT	5.78				
DT	-1.74				
RT*IDC	8.56	0.0024	0.0022	0.0023	0.0021
RT*CC	-0.72	-0.0321	-0.0319	-0.0318	-0.0316
RT*T	-1.88	-0.0033	-0.0033	-0.0033	-0.0033
RT*PT	1.05				
RT*DT	-0.37				
IDC*CC	-4.09	-0.1090	-0.1097	-0.1096	-0.1093
IDC*T	6.71	0.0072	0.0072	0.0072	0.0072
IDC*PT	-0.012				
IDC*DT	0.32				
CC*T	0.10	0.0167	0.0166	0.0169	0.0171
CC*PT	-0.17				
CC*DT	-0.24				
T*PT	0.17				
T*DT	-0.15				
RT^2	-0.14				
IDC^2	-3.23	-0.0016	-0.0015	-0.0019	-0.0018
CC^2	-0.26	-0.00005	-0.00005	-0.00005	-0.00005
T^2	0.61	2.4291	2.4289	2.4287	2.4283
R^2_{adj} (%)	94.40	99.52	98.14	99.48	98.01
R^2_{cv} (%)	92.35	97.79	96.61	97.52	96.52
Adeq. precision	42.97	87.16	69.71	85.42	68.59
SD	4.03	1.04	1.68	1.15	1.76
Mean	71.02	68.76	81.12	66.24	80.35
CV	5.68	3.42	4.28	3.69	4.52
PRESS	2644.38	4679.36	3842.24	4371.22	3689.16

*CC: Adsorbent concentration (g L^{-1}); DE: Decolorization efficiency (%); DT: Dye type; IDC: Initial dye concentration (mg L^{-1}); PT: Process type; RT: Reaction time (min); and T: Temperature (^oC). *Binary process was used by which both process type with two levels and dye type with two levels are included*

Table 5. Best-fit artificial neural networks (ANNs) of decolorization efficiency (%) for RY145 as a function of reaction time (min), initial dye concentration (mg L^{-1}), initial adsorbent concentration (g L^{-1}), temperature (°C), process type, and dye type.

Model	Structure	Topology	RMSE	MAE	R^2 value		
					Training (70%)	Cross-validation (15%)	Independent validation (15%)
ANN6	8*1	SLP	7.80	0.065	98.18	98.11	92.53
ANN45	3*24*1	MLP	2.04	0.012	99.67	99.03	98.57
ANN47	5*3*1		2.69	0.019	99.82	99.09	97.38

MAE: Mean absolute error; MLP: Multilayer perceptron; RMSE: Root mean square error; and SLP: Single layer perceptron

Table 6. Validation of response surface methodology (RSM)-optimized operating conditions for predicted and experimental decolorization efficiencies (DE, %)

DT	RT	IDC	CC	T	PT	Desirability	DE (Predicted)	DE (Experimental)
RY145	119.99	225.41	1.41	50.00	Adsorption	0.99	99.99	98.73±0.26
RY145	76.98	233.20	1.37	35.42	UAA	1	99.99	99.89±0.02
RB19	120.00	226.50	1.50	50.00	Adsorption	0.97	97.84	95.22±0.32
RB19	79.40	254.29	1.44	49.37	UAA	1	99.99	96.66±0.51

CC: Adsorbent concentration (g L^{-1}); DT: Dye type; IDC: Initial dye concentration (mg L^{-1}); PT: Process type; RT: Reaction time (min); and T: Temperature (°C). Desirability ranging from 0 to 1 refers to the confirmation process by which one out of 100 runs of the optimal conditions generated is randomly selected for experiments to be replicated, and results are compared in terms of DE

3.7. Comparison of adsorption and UAA with CC to those with different adsorbents

The UAA treatment with the CC adsorbent used in this study was compared to the other adsorption and UAA treatments with such adsorbents as poly nanotubes, dehydrated wheat bran carbon, dehydrated peanut hull, and activated carbon under the similar initial Methylene Blue concentrations in terms of decolorization efficiency and adsorbent capacity in Table 7. From Table 7, it can be inferred that UAA with CC appears to be a promising wastewater treatment process. However, it should be noted that operating costs also need to be considered together with decolorization efficiency for comparison. For example, CC is an abundant, and thus, low-cost by-product in Turkey, thus rendering the operating cost of UAA more attractive to the other absorbents.

Table 7. Comparison of adsorption and ultrasound-assisted adsorption (UAA) with dehydrated cottonseed cake (CC) used in this study to those with other adsorbents published in related literature under the similar initial dye (Methylene Blue) (IDC) concentration in terms of decolorization efficiency (DE)

Decolorization process	IDC (mg L^{-1})	RT (min)	DE (%)	References
Adsorption with PN	20	15	95	Chen *et al*., (2015)
Adsorption with DWBC	200	1800	99.84	Ozer and Dursun, (2007)
Adsorption with DPH	100	1500	97.5	Ozer *et al*., (2007)
	150	1500	81.8	
	200	1500	68.2	
	250	1500	56.6	
Adsorption with CC	50	120	77.28	This study
	250	120	71.05	
UAA with CC	50	15	87.31	
	250	15	80.52	
UAA with AC	50	15	99	Sayan and Edecan, (2008)

AC: Activated carbon; DPH: Dehydrated peanut hull; DWBC: Dehydrated wheat bran carbon; and PN: Poly nanotubes

4. Conclusions

RSM using BBD was applied to the optimization of decolorization efficiencies for RY145 and RB19 by adsorption and UAA in a batch process. The decolorization efficiencies achieved under RSM-optimized conditions varied between 95.22% with adsorption for RB19 and 99.99% with UAA for RB19 and RY145. When validated using the replication experiments, our results confirmed the accuracy of RSM optimization of adsorption and UAA operating conditions. The best-fit MNLR and ANN models identified the significantly linear, quadratic and interaction effects of the predictors. Our results pointed to the better performance of the ANNs than the MNLR models in elucidating changes in the decolorization efficiencies.

Acknowledgements

The authors would like to thank the Scientific Research Projects Unit of Abant Izzet Baysal University (AIBU) (Projects no: 2015.09.02.920; 2016.09.02.1035; 2016.09.02.1006; 2016.09.02.1007) for financial supports.

Declaration of conflicting interest

The authors do not have any potential conflicts of interest to declare.

References

Buyukada M. (2015), Removal of Yellow F3R, Di Maria Brilliant Blue R and Reactive Brilliant Red M-3BE from aqueous Solutions by a rapid and efficient ultrasound-assisted process with a novel biosorbent of cottonseed cake: statistical modeling, kinetic and thermodynamic studies, *Arabian Journal for Science and Engineering*, **40**(8), 2153-2168.

Buyukada M. (2016), Co-combustion of peanut hull and coal blends: artificial neural networks modeling, particle swarm optimization and Monte Carlo simulation, *Bioresource Technology*, **216**, 280-286.

Buyukada M. (2017), Probabilistic uncertainty analysis based on Monte Carlo simulations of co-combustion of hazelnut hull and coal blends: Data driven modeling and response surface optimization, *Bioresource Technology*, **225**, 106-112.

Buyukada M. and Evrendilek F. (2016a), Modeling efficiency of dehydrated sunflower seed cake as a novel biosorbent to remove a toxic azo dye, *Chemical Engineering Communications*, **203**(6), 746-757.

Buyukada M. and Evrendilek F. (2016b), Modeling ultrasound-assisted decolorization efficiency of Reactive Blue 19 and Reactive Yellow 145 from aqueous solutions by cottonseed cake, *Fresenius Environmental Bulletin*, **25**(3), 692-705.

Chen Z., Zhang J., Fu J., Wang M., Wang X., Han R. and Xu Q. (2015), Adsorption of methylene blue onto poly(cyclotriphosphazene-co-4,4′-sulfonyldiphenol) nanotubes: Kinetics, isotherm and thermodynamics analysis, *Journal of Hazardous Materials,* **273**, 263–271.

Dincer A.R., Gunes Y., Karakaya N. and Gunes E. (2007), Coal-based bottom ash (CBBA) waste material as adsorbent for removal of textile dyestuffs from aqueous solution, *Journal of Hazardous Materials,* **141**, 529–535.

Gong R.M., Ding Y., Lie M., Yang C., Liu H.J. and Sun Y.Z. (2005), Utilization of powdered peanut hull as biosorbent for removal of anionic dyes from aqueous solution, *Dyes and Pigments*, **64,** 187–192.

Guo W.Q., Ding J., Cao G.L., Ren N.Q. and Cui F.Y. (2011), Treatability study of using low frequency ultrasonic pretreatment to augment continuous biohydrogen production, *International Journal of Hydrogen Energy,* **36**, 14180–14185.

Hamdaoui O., Chiha M. and Naffrechoux E. (2008), Ultrasound-assisted removal of malachite green from aqueous solution by dead pine needles, *Ultrasonics Sonochemistry,* **15**, 799–807.

Korkut O., Sayan E., Lacin O. and Bayrak B. (2010), Investigation of adsorption and ultrasound assisted desorption of lead (II) and copper (II) on local bentonite: a modelling study, *Desalination,* **259**, 243–248.

Liu X., Yang Y., Shi X. and Li K. (2015), Fast photocatalytic degradation of methylene blue dye using a low-power diode laser, *Journal of Hazardous Materials,* **283**, 267–275.

Mohan S.V., Rao N.C., Prasad K.K. and Karthikeyan J. (2002), Treatment of simulated Reactive Yellow 22 (Azo) dye effluents using *Spirogyra* species, *Journal of Waste Management*, **22**, 575-582.

Onat A.T., Gumusdere T.H., Guvenc A., Donmez G. and Mehmetoglu U. (2010), Decolorization of textile azo dyes by ultrasonication and microbial removal, *Desalination,* **255**, 154–158.

Ozer A. and Dursun G. (2007), Removal of methylene blue from aqueous solutions by dehydrated wheat bran carbon, *Journal of Hazardous Materials*, **146**, 262–269.

Ozer D., Dursun G. and Ozer A. (2007), Methylene blue adsorption from aqueous solutions by dehydrated peanut hull, *Journal of Hazardous Materials,* **144**, 171–179.

Ren X.L., Lai X.H., Zhu K.J., Sun Y. and He D.L. (2016), Removal of acid turquoise blue 2G from aqueous solution by adsorbent derived from sludge and straw: kinetic, isotherm and thermodynamic study, *Desalination and Water Treatment,* **57**(1), 440–448.

Sahinkaya S. (2013), COD and color removal from synthetic textile wastewater by ultrasound assisted electro-Fenton oxidation process, *Journal of Industrial Chemistry,* **19**, 601–605.

Sayan E. and Edecan M.E. (2008), An optimization study using response surface methods on the decolorization of reactive blue 19 from aqueous solution by ultrasound, *Ultrasonics Sonochemistry*, **15**, 530–538.

Tanyildizi M.S. (2011), Modeling of adsorption isotherms and kinetics of reactive dye from aqueous solution by peanut hull, *Chemical Engineering Journal*, **168**, 1234–1240.

Yang S.S., Guo V.Q., Zhou X.J. Meng Z.H., Liu B. and Ren N.Q. (2011), Optimization of operating parameters for sludge process reduction under alternating aerobic/oxygen-limited conditions by response surface methodology, *Bioresource Technology,* **102**, 9843–9851.

Yargic A.S., Yarbay-Sahin R.Z., Ozbay N. and Onal E. (2015), Assessment of toxic copper (II) biosorption from aqueous solution by chemically-treated tomato waste, *Journal of Cleaner Production,* **88**, 152–159.

Zhou X.J., Guo W.Q., Yang, S.S. and Ren N.Q. (2013), Ultrasonic-assisted ozone oxidation process of triphenyl methane dye degradation: evidence for the promotion effects of ultrasonic on malachite green decolorization and degradation mechanism, *Bioresource Technology,* **128**, 827–830.